

Thermal Stability of Retained Austenite in Bainitic Steel: an *in situ* study

BY A. SAHA PODDER, I. LONARDELLI, A. MOLINARI AND H. K. D. H.
BHADESHIA

University of Cambridge
Materials Science and Metallurgy
Pembroke Street, Cambridge CB2 3QZ, U. K.

University of Trento
Materials Engineering and Industrial Technologies
Via Mesiano 77, 38123 Trento, Italy

Abstract

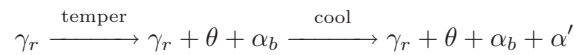
The tempering of two-phase mixtures of bainitic ferrite and carbon-enriched retained austenite has been investigated in an effort to separate the reactions that occur at elevated temperatures from any transformation during cooling to ambient conditions. It is demonstrated using synchrotron X-radiation measurements, that the residue of austenite left at the tempering temperature partly decomposes by martensitic transformation when the sample is cooled. It is well-established in the published literature that films of retained austenite are better able to resist stress or strain-induced martensitic transformation than any coarser particles of austenite. In contrast, the coarser austenite is more thermally stable than the film form because of its lower carbon concentration.

1. Introduction

Carbide-free bainitic steels in which a proportion of the microstructure consists of a mixture of bainitic ferrite and carbon-enriched retained austenite are now well-established as some of the most sophisticated engineering materials. Applications range from the formable alloys for the automobile industry (Matsumura et al., 1987a,b), ductile cast-irons (Rundman and Klug, 1982), railway lines (Bhadeshia, 2007; Yates, 1996) and armour (Bhadeshia, 2005; Caballero and Bhadeshia, 2004). There also exist many variants of the basic concept which are the subject of intense research from both a fundamental and applied perspective (Caballero et al., 2010; Menapace et al., 2009; Saha Podder et al., 2007; Stone et al., 2008; Sugimoto, 2009; Yi et al., 2010). Structures of this kind, but on a scale finer than carbon nanotubes, can now be produced on a commercial scale, as reviewed recently (Bhadeshia, 2010).

One role of retained austenite is to enhance the ductility of the steel (DeCooman, 2004; Jacques, 2004). It transforms under the influence of stress and strain and thereby increases the work-hardening rate sufficiently to delay plastic instabilities; the transformation strain itself plays a minor role in this process (Bhadeshia, 2002). The mechanical stability of the austenite is well understood and serves as a mechanism for controlling the properties.

However, there are circumstances in which the steel, after it is produced with the desired microstructure, is subjected temporarily to an elevated temperature in excess of 400°C; one example is the galvanising treatment where the steel passes through a bath of a molten zinc-rich alloy. Another case is where aeroengine shafts, which do not experience high temperatures during service, have to be heated to temperatures in excess of 500°C in order to apply corrosion-resistant coatings. It is possible that the thermal stability of the austenite would not in these cases be sufficient, leading to its decomposition into a thermodynamically more stable mixture of ferrite and cementite. Bearing this in mind, Saha Podder and Bhadeshia (2010) investigated the kinetics of the decomposition of carbon-enriched retained austenite as a function of a tempering heat treatment, using a combination of microscopy and X-ray diffraction on samples cooled to ambient temperature following the excursion to elevated temperatures. When the mixture of bainitic ferrite and retained austenite (γ_r) is heated to the tempering temperature, some of the austenite undergoes thermal decomposition into a mixture of bainitic ferrite (α_b) and cementite (θ) but a proportion of the remainder may decompose into martensite (α') during cooling to ambient temperature. It follows that the quantities measured are a combination of two decomposition reactions rather than just the influence of thermal decomposition:



where the amount of austenite is reduced at each stage of the process.

The purpose of this work was to characterise separately the two reactions of thermal decomposition and the transformation to martensite during cooling from the tempering temperature, by using high-energy synchrotron X-rays to conduct *in situ* experiments. The work is a part of basic research in which we hope to increase the thermal stability of bulk nanostructured steels (Bhadeshia, 2010).

2. Experimental Procedure

An Fe-0.39C-4.09Ni-2.05Si wt% alloy was prepared as a 20 kg vacuum induction melt from high purity base materials; this material has previously been studied to establish the relationship between structure and properties for mixtures of bainitic ferrite and retained austenite, with the latter phase present both as blocks and films (Bhadeshia and Edmonds, 1983a,b). The silicon content ensures that cementite does not precipitate during the formation of bainite. The equilibrium phase fractions calculated using MTDATA and associated TCFE database (NPL, 2006) and assuming that austenite, ferrite and cementite are permitted phases, are shown in Fig. 1a.

Alloy preparation methods are given in the original work, but cylindrical samples, 12 mm long and 8 mm diameter, were prepared for use on a *Thermecmaster* thermomechanical simulator. The machine is equipped with an environmental chamber which was evacuated to 2×10^{-4} torr during austenitisation. The sample is induction heated and cooling is carried out by blowing helium directly onto the specimen surface. The heat treatment used is illustrated in Fig. 1b. Following isothermal transformation, some samples were tempered at 400°C for 30 to 120 min for conventional X-ray measurements using a Philips vertical diffractometer with unfiltered CuK_α radiation, and the instrument operated at 40 kV and 40 mA. A continuous scanning mode was chosen with the rate of $0.05^\circ \text{ s}^{-1}$ over the angular width of $2\theta = 30\text{-}150^\circ$ with collecting time of 16.65 s at each step. A secondary monochromator in the form of curved graphite is used to eliminate CuK_β radiation. A divergent slit of 1° and receiving slit of 0.2 mm was used. Four discs, each with a diameter of 8 mm, were sliced from the specimen after the heat treatments. Each sample was polished using the standard metallographic techniques and was etched with 2% nital and were used for X-ray analysis. Peak positions and phases were identified using X'Pert HighScore Plus software. The fraction of retained austenite was evaluated using Rietveld refinement (McCusker et al., 1999; Rietveld, 1967, 1969).

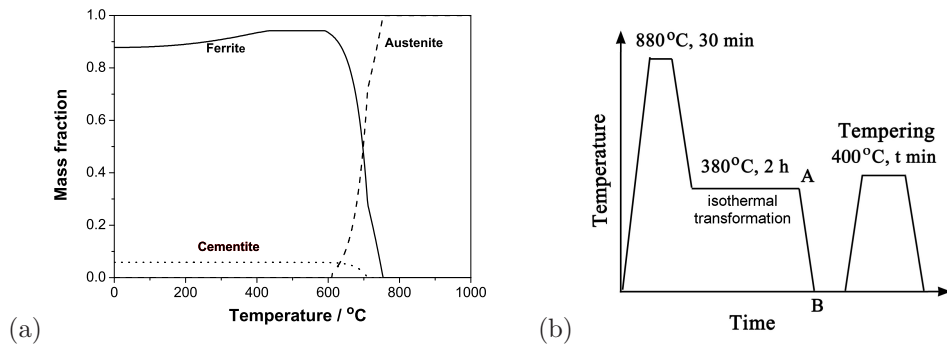


Figure 1. (a) Calculated equilibrium phase fractions. (b) The heat treatment schedule.

Another set of isothermally transformed samples with the microstructure of bainitic ferrite and austenite was retained without tempering in order to study the process as it happens, using synchrotron X-radiation as described in the section that follows. For this purpose cylindrical samples of 10 mm length and 0.8 mm diameter were machined from the isothermally transformed materials. The tempering was carried out on the synchrotron facility at 400°C using a hot air blower whilst the sample is exposed to an X-ray beam of monochromatic wavelength 0.50247 \AA and a beam size of 10 mm horizontal \times 0.6 mm vertical. The temperature in the blower was calibrated by monitoring the thermal expansion of a platinum specimen. The Swiss-Norwegian Beam Line BM01 at the European Synchrotron Radiation Facility in Grenoble, France was used for this purpose. A robust 2-circle diffractometer was available for high resolution powder diffraction measurements (Fig. 2). Each circle has a high precision encoder mounted directly on the rotation axis. This Bragg-Brentano diffractometer works in transmission geometry. The 13 element Ge detector has 6 fast counting chains to have for each analysis, six complete patterns

collected simultaneously, with an offset in $2\theta = 1.1^\circ$, in order to reduce the total data collection time to a minimum.

Diffraction spectra for each sample were collected at room temperature prior to tempering at 400°C for further collection of spectra. In both cases the full width half maximum resolution was 0.01° . The 2θ ranges were 9 to 37.5° at ambient temperature and 11.5 to 22.5° during tempering with a total acquisition time of 5 min for each spectrum. Heating and cooling were performed rapidly by moving the rotating sample above the air blower. A reference sample of silicon (NIST SRM-640c) was used to calibrate the instrument and the peak-broadening functions for the integrations. The diffraction data were analysed using the Rietveld method as implemented in the program package MAUD (Materials Analysis Using Diffraction) (Lutterotti et al., 1997).

Three separate tempering sequences were carried out as shown in Fig. 3, all with the tempering temperature fixed at 400°C . Treatments–I and II involved two stages, the first consisting of 30 and 45 min of tempering respectively, followed by quenching to room temperature where diffraction data were also collected. The purpose was to observe the change in the carbon content of retained austenite after partial martensitic transformation during cooling (Saha Podder and Bhadeshia, 2010). In the second stage, the samples were reheated to the tempering temperature and held for the specified period. Finally the samples were quenched to room temperature. In treatment–III there was no interruption during the period of 180 min, afterwards the sample was quenched to room temperature.

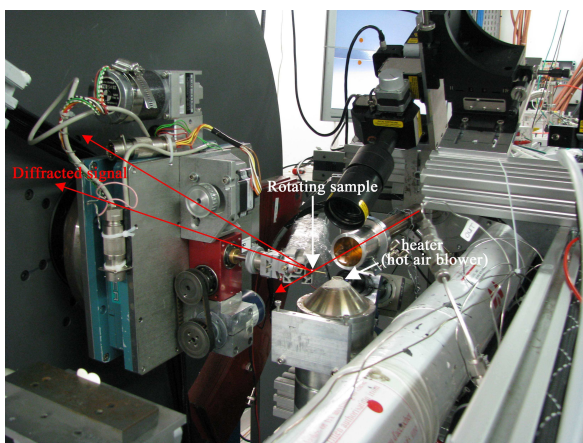


Figure 2. Sample assembly mounted at beam line with hot air blower positioned underneath.

3. Results

The microstructure following isothermal transformation at 380°C for 2 h consists of a mixture of bainitic ferrite and carbon-enriched retained austenite as shown in Fig. 4, which also illustrates the two forms of austenite, blocky and film-like. This structure was then tempered within the synchrotron instrument with data collected

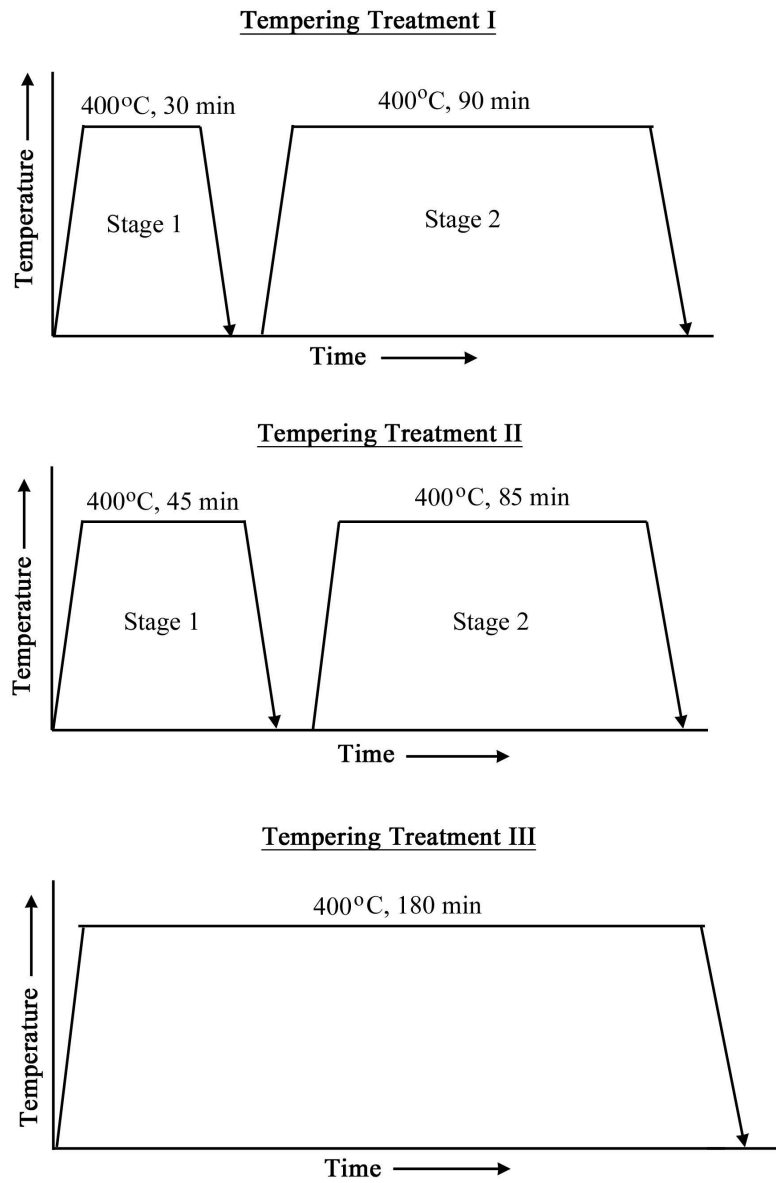


Figure 3. Tempering treatments carried out using synchrotron X-radiation. Arrows indicate the quench to room temperature.

every five minutes. Fig. 5 shows the change in retained austenite content during tempering. The zero tempering time corresponds to the sample in its isothermally transformed state with the austenite fraction measured at room temperature, to be 0.19. This graph also shows low-energy X-ray diffraction data measured at ambient

temperature for comparison purposes; these data show a lower fraction of austenite than that which the synchrotron experiments suggest existed at the tempering temperature. To assess this discrepancy, the synchrotron sample was characterised after the 120 min temper, when it cooled to ambient temperature, using conventional X-ray diffraction; this particular measurement is represented as a circle on Fig. 5 and shows that some of the austenite which existed at the tempering temperature decomposes on cooling the sample to ambient temperature. It was confirmed using scanning electron microscopy that decarburisation did not occur during the tempering heat treatment, as shown by the absence of ferrite and the uniformity of the microstructure as the surface is approached in Fig 6.

Conventional X-rays have a lower penetration than the synchrotron radiation and hence might lead to an underestimation of retained austenite content if the sample decarburised during tempering at 400°C. It is estimated that the penetration depth of X-rays in Fe(γ) with CuK α target varies from 0.5-1.7 μm for the angle of incidence (2θ) between 20°-150° (Marques et al., 2005). In case of synchrotron radiation the depth of penetration lies in the range of 68 to 75 μm for the wavelength of 0.5 Å (Dudley et al., 1989). A further experiment in which conventional X-ray samples were tempered for more than 30 min, and chemically polished did not lead to different values for the retained austenite content, so the observed differences between the two techniques cannot be attributed to surface effects.

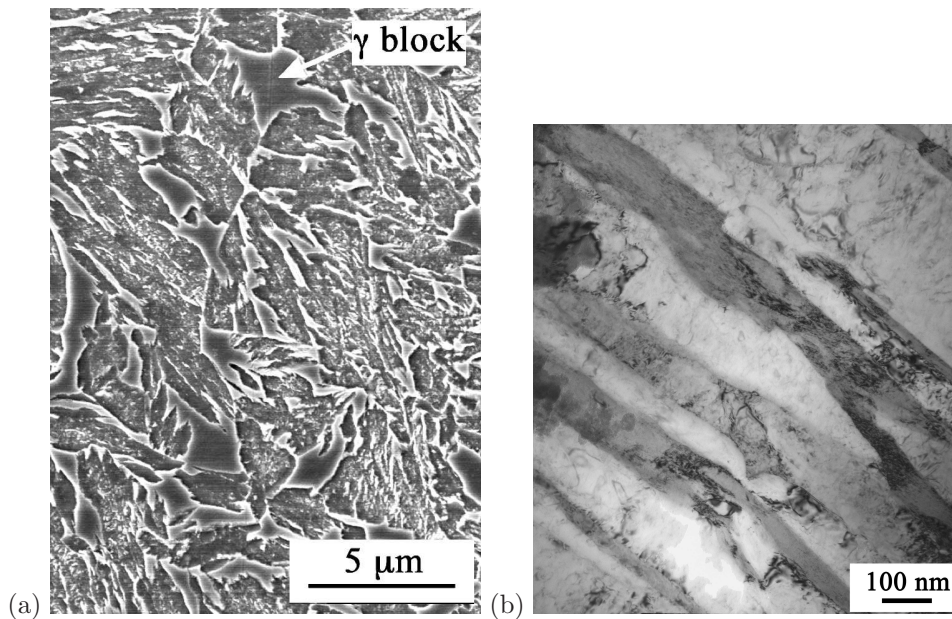


Figure 4. Sample isothermally transformed at 380°C. (a) Scanning electron micrograph illustrating the blocky regions of austenite. (b) Transmission electron micrograph showing bainitic ferrite with intervening films of retained austenite.

We have emphasised that there are two morphologies of austenite present in the microstructure, the blocks and thin films trapped between the platelets of bainitic ferrite; the films are known from independent experiments to be more mechanically

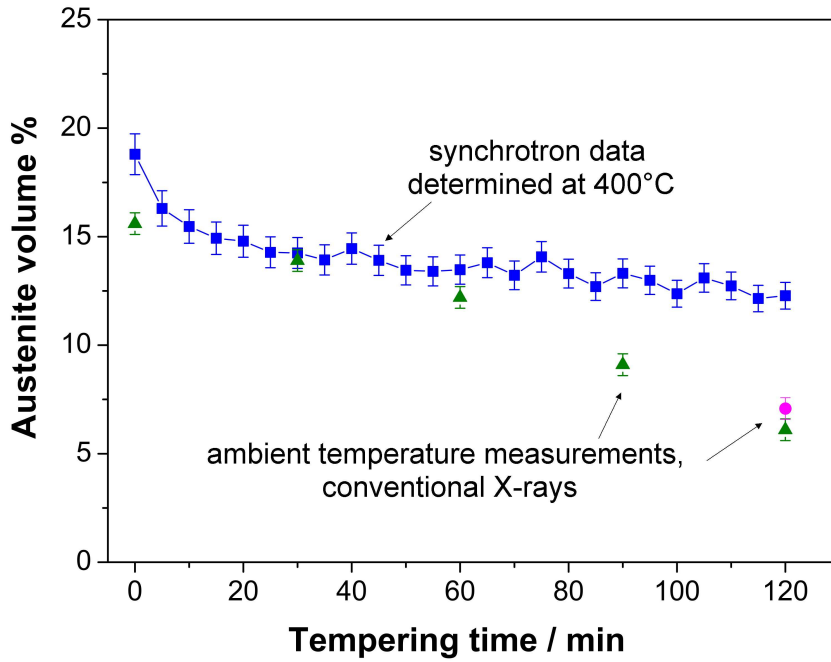


Figure 5. Retained austenite content as a function of time following tempering treatment-I.

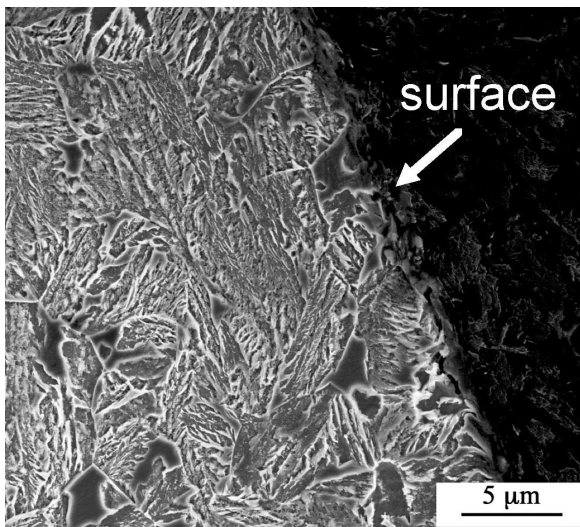


Figure 6. Scanning electron micrograph showing microstructure at the edge of the sample after tempering treatment-I.

stable to martensitic transformation (Bhadeshia and Edmonds, 1983a) and richer in carbon (Bhadeshia and Waugh, 1982; Self et al., 1981). The two kinds of austenite differ in terms of crystallite size and lattice parameter with the consequence that peaks in X-ray diffraction spectra show asymmetry and hence can be deconvoluted as shown in Fig. 7. If it can be assumed that the film austenite contains a larger

concentration of carbon, then the broader of the two peaks corresponds to the film variety since it should have a larger lattice parameters and hence smaller Bragg angle θ ; the breadth of that peak is consistent with the finer scale of the film austenite. The axial divergence was not considered for the analysis of synchrotron results because in the studied material, axial broadening does not contribute to the peak asymmetry. This was confirmed using a standard silicon sample which did not exhibit peak asymmetry Fig. 8.

The changes in quantities of both the forms of austenite during tempering treatment–I are plotted in Fig. 9. The plot shows that blocky austenite always maintains a larger volume fraction as compared with the films. The volume fraction of both blocky and film austenite has decreased with the progress of tempering, but this reduction is gradual for the blocky constituent whereas there is sharp decrease in fraction of the film type in the initial stage, after which there is little change. Similarly volume% of both the austenite variants were analysed during treatment–II (Fig. 10). The trend is similar with treatment–I. The only difference with the earlier graph is that here both the constituents reduce gradually as the tempering time elapses. The deconvolution of individual constituents of the austenite intensity is sensitive to the profile fitting.

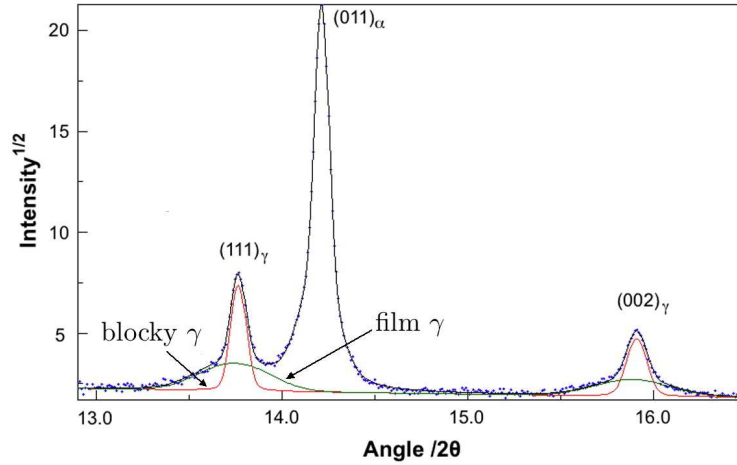


Figure 7. The figure shows deconvolution of two different types of austenite.

The lattice parameter of untransformed austenite at the tempering temperature T was calculated from the room temperature (298 K) value using the thermal expansion coefficient, e_γ :

$$a_\gamma^T = a_\gamma^{298} [1 + e_\gamma(T - 298)] \quad (3.1)$$

where T is the temperature in K and a_γ represents the lattice parameter of austenite. The thermal expansion coefficient of austenite considered in these calculations was $e_\gamma = 2.065 \times 10^{-5} \text{ K}^{-1}$ (Takahashi, 1992). The expansion coefficient is necessary in order to convert a_γ measured at the tempering temperature into a value

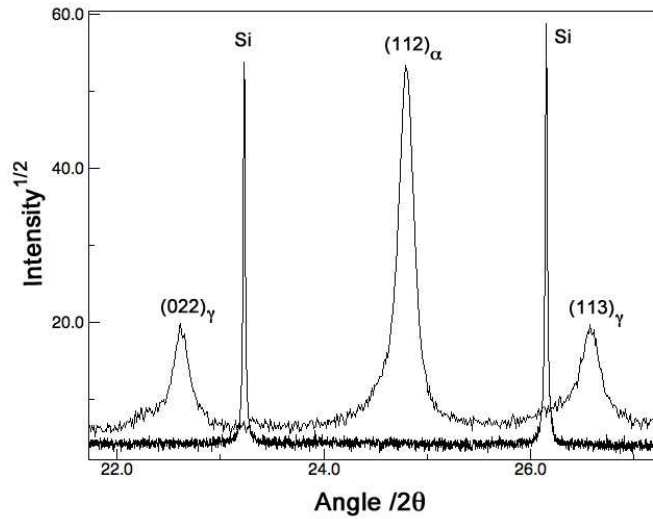


Figure 8. Superimposed peaks from the standard silicon sample.

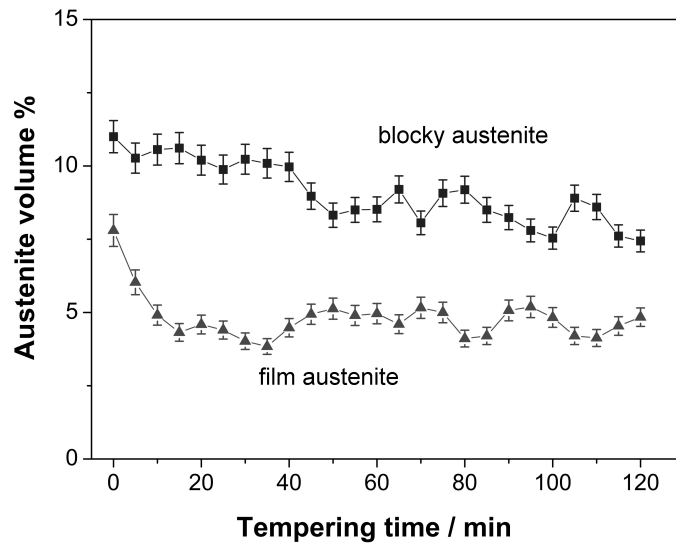


Figure 9. Change in amounts of blocky and film-type austenite at 400°C during tempering treatment-I.

at ambient temperature, in order to permit the composition of the austenite to be estimated. The carbon content of retained austenite was calculated using the relationship between lattice parameter and chemical composition reported by (Dyson and Holmes, 1970). This expression was selected as being the most complete in terms of the contribution of different solutes to the austenite lattice parameter and its use has been validated due to reasonable agreement with atom probe mea-

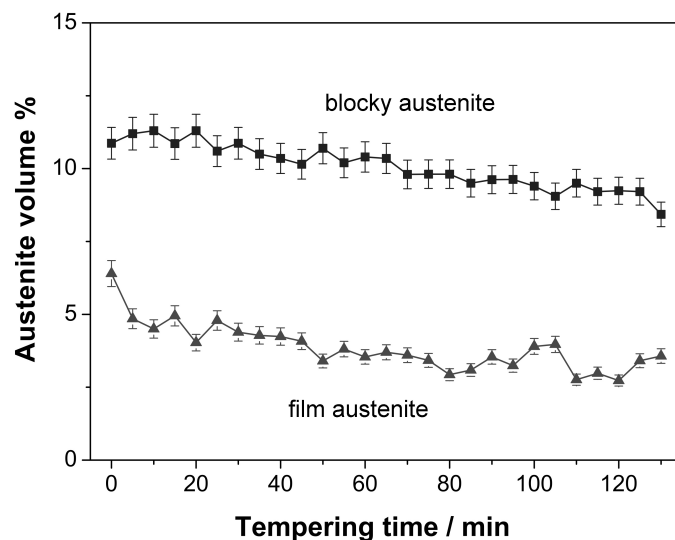


Figure 10. Change in amounts of austenite constituents at 400°C, measured during tempering treatment-II.

surements (Caballero et al., 2007; Garcia-Mateo and Caballero, 2005; Peet et al., 2004).

Assuming that the film austenite is richer in carbon, the deduced concentrations of the two forms of austenite are plotted in Fig. 11a,b. The consistently greater carbon concentration in the films explains why they decompose relatively rapidly (Fig. 9) because the driving force for cementite precipitation is greater. Therefore, although the films are more stable to transformation during cooling or under the influence of stress, they are less stable than the lower carbon blocks of austenite during tempering heat treatment.

During tempering treatments I and II, the specimens were quenched to room temperature after stage 1. Fig. 11 shows that on both the occasions the carbon content of film and blocky austenite has increased from the value measured at 400°C before and after quenching. This is only possible when the unstabilised austenite transforms to martensite during cooling, resulting in increasing carbon content of the remaining austenite (Saha Podder and Bhadeshia, 2010). The room temperature results after stage 2 also showing similar behaviour because there is still 12.3 volume % of austenite retained in the sample.

The progress of transformation during *in situ* tempering can be accomplished through the change in total austenite content, Fig. 12. The decomposition reaction is sluggish after 1 h, as a result the amounts of austenite remained in the structure are similar following treatments II and III.

Synchrotron X-ray patterns of untempered material and after tempering for 30 min and 120 min, obtained at room temperature, are shown in Fig. 13. The effect of tempering can be observed from the (002) peak of austenite. Low-energy

X-ray results are shown in Fig. 14, which shows faster reduction of austenite fraction through the decrease in austenite peaks intensity. After isothermal transformation the material contained 0.16 ± 0.01 and 0.19 ± 0.01 volume fraction of austenite measured using low and high-energy X-ray diffraction respectively.

The microstructure after tempering is shown in Fig. 15a. The amount of austenite retained in the structure after 2 h of tempering was 12.3 volume%. The blocky austenite can be clearly observed in the microstructure primarily at the grain boundaries, it may be noted that the blocky austenite present in the structure in larger volume as described in Figs. 9 and 10. Transmission electron microscopy examination revealed presence of cementite particles in the tempered specimen. Fig. 16a shows cementite (θ) precipitates at the grain boundaries and the corresponding electron diffraction pattern confirms the cementite phase.

4. Summary

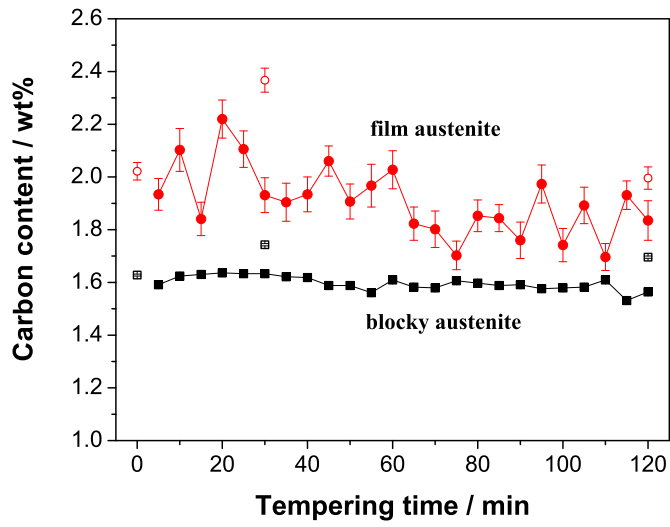
Some clear deductions can be made from the discrepancies between the synchrotron austenite measurements conducted at the tempering temperature, and the smaller quantities detected using low energy X-ray radiation following the cooling of the samples to ambient temperature (Fig. 5). It has been demonstrated that the difference cannot be explained in terms of decarburisation.

The results therefore indicate that some of the austenite residue left at the tempering temperature decomposes by martensitic transformation during cooling to ambient temperature. This is not surprising given that the precipitation of carbides reduces the stability of the austenite to martensitic transformation (Saha Podder and Bhadeshia, 2010).

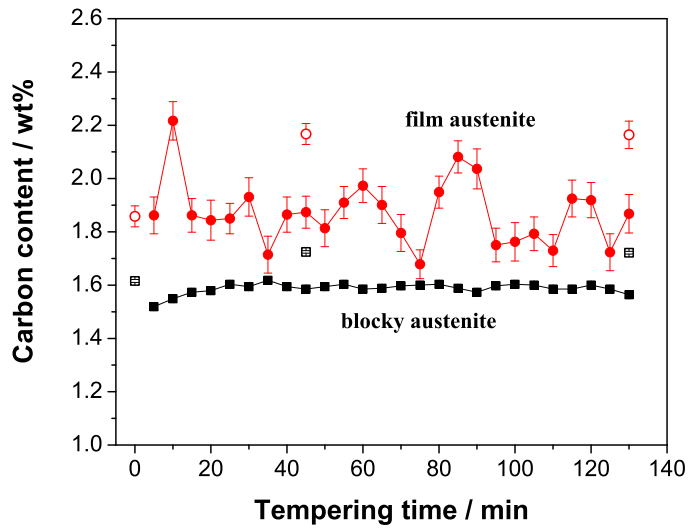
An interesting result is that although the films of austenite are well-known to be more stable than the blocks to martensitic transformation, whether induced by cooling or by the application of stress, the films are less stable when it comes to decomposition during tempering by the precipitation of cementite. The reason for this is straightforward, that the films are richer in carbon and there is therefore a greater driving force for cementite precipitation.

Acknowledgments

We are grateful to the Cambridge Commonwealth Trust, the Hinduja Foundation, British Petroleum for funding this work and to Tata Steel Ltd. for providing study leave. We appreciate access to the synchrotron beam line BM01 at ESRF, BM01 and gratefully acknowledge assistance from Dr H. Emerich during data collection. This work was partially supported by the European Union, Marie Curie Actions, Marie-Curie 7th Framework Programme, the Trentino programme research.



(a)



(b)

Figure 11. Carbon content of retained austenite obtained during *in situ* tempering for (a) treatment-I and (b) treatment-II. Open markers represent the results from room temperature measurements.

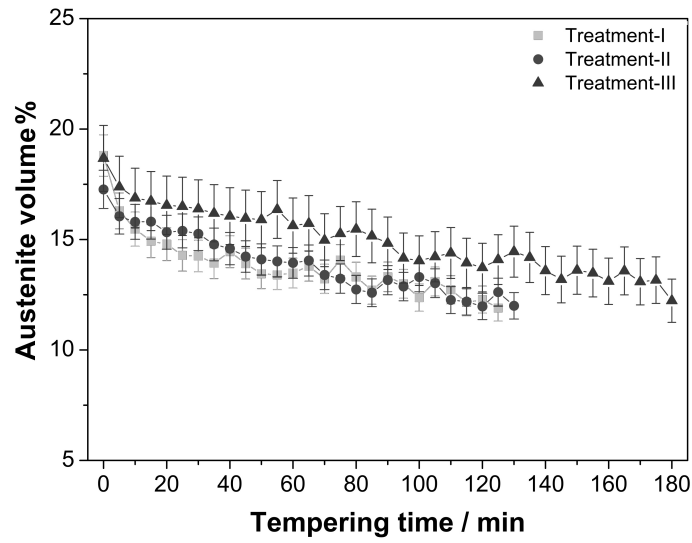


Figure 12. Measured volume% of retained austenite as a function of tempering time for three different tempering treatments.

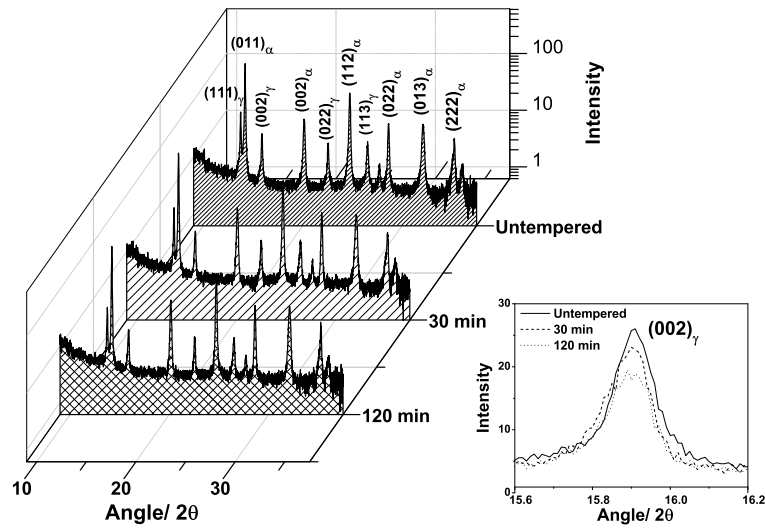


Figure 13. The plot showing synchrotron X-ray diffraction results after tempering treatment-I measured at room temperature.

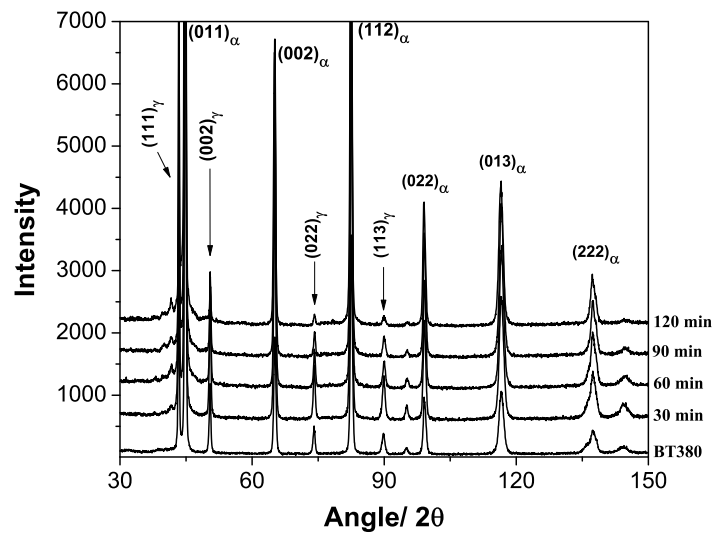
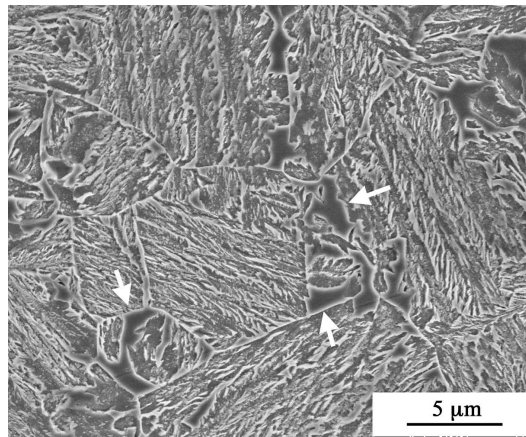
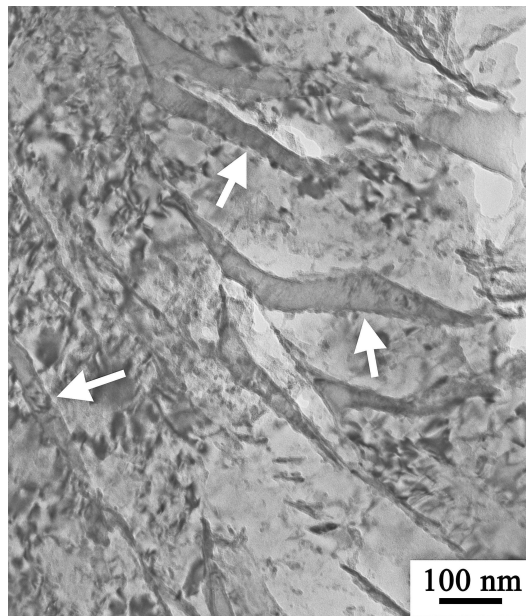


Figure 14. Results of low-energy X-ray diffraction. Isothermal transformation at 390°C (BT380) and followed by tempering at 400°C for different durations.

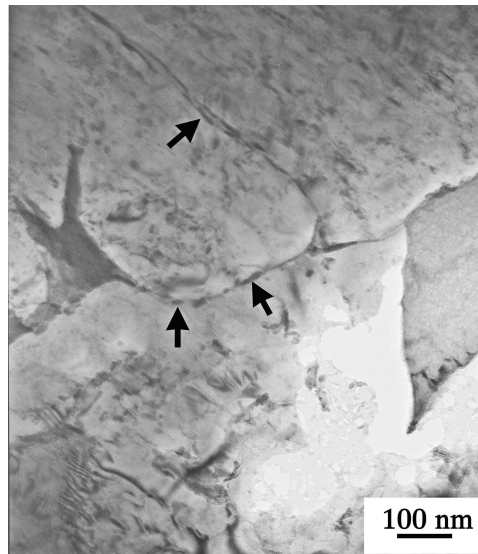


(a)

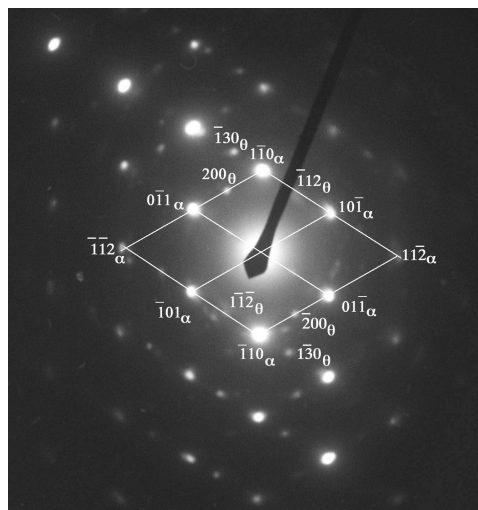


(b)

Figure 15. (a) Scanning electron micrograph of the tempered sample after tempering treatment-I, showing retained austenite (arrowed) present in the microstructure even after 2 h of tempering. (b) Corresponding transmission electron micrograph showing retained austenite marked with arrows.



(a)



(b)

Figure 16. (a) Transmission electron micrograph showing precipitation of fine cementite particles (arrowed) in the tempered specimen, tempered using *Thermecmaster* at 400°C for 30 min. (b) Electron diffraction pattern obtained from the precipitates.

References

- Bhadeshia, H. K. D. H., 2002. TRIP-assisted steels? *ISIJ International* 42, 1059–1060.
- Bhadeshia, H. K. D. H., 2005. Large chunks of very strong steel. *Materials Science and Technology* 21, 1293–1302.
- Bhadeshia, H. K. D. H., 2007. Steels for rails. In: *Encyclopedia of Materials Science*. Pergamon Press, Oxford, Elsevier Science, pp. 1–7.
- Bhadeshia, H. K. D. H., 2010. Nanostructured bainite. *Proceedings of the Royal Society of London A* 466, 3–18.
- Bhadeshia, H. K. D. H., Edmonds, D. V., 1983a. Bainite in silicon steels: a new composition property approach i. *Metal Science* 17, 411–419.
- Bhadeshia, H. K. D. H., Edmonds, D. V., 1983b. Bainite in silicon steels: a new composition property approach ii. *Metal Science* 17, 420–425.
- Bhadeshia, H. K. D. H., Waugh, A. R., 1982. Bainite: An atom probe study of the incomplete reaction phenomenon. *Acta Metallurgica* 30, 775–784.
- Caballero, F. G., Bhadeshia, H. K. D. H., 2004. Very strong bainite. *Current Opinion in Solid State and Materials Science* 8, 251–257.
- Caballero, F. G., Miller, M. K., Babu, S. S., Garcia-Mateo, C., 2007. Atomic scale observations of bainite transformation in a high carbon high silicon steel. *Acta Materialia* 55, 381–390.
- Caballero, F. G., Miller, M. K., Garcia-Mateo, C., 2010. Tracking solute atoms during bainite reaction in a nanocrystalline steel. *Materials Science and Technology* 26, 889–898.
- DeCooman, B., 2004. Structure–properties relationship in TRIP steels containing carbide-free bainite. *Current Opinion in Solid State and Materials Science* 8, 285–303.
- Dudley, M., Wu, J., Yao, G. D., 1989. Determination of penetration depths and analysis of strains in single crystals by white beam synchrotron X-ray tomography in grazing Bragg-Laue geometries. *Nuclear Instruments and Methods in Physics Research B* 40/41, 388–392.
- Dyson, D. J., Holmes, B., 1970. Effect of alloying additions on the lattice parameter austenite. *Journal of the Iron and Steel Institute* 208, 469–474.
- Garcia-Mateo, C., Caballero, F. G., 2005. Role of retained austenite on tensile properties of steels with bainitic microstructures. *Materials Transactions* 46, 1839–1846.
- Jacques, P. J., 2004. Transformation-induced plasticity for high strength formable steels. *Current Opinion in Solid State and Materials Science* 8, 259–265.

- Lutterotti, L., Matthies, S., Wenk, H. R., Shultz, A. S., Richardson, J. W., 1997. Combined texture and structure analysis of deformed limestone from time-of-flight neutron diffraction spectra. *Journal of Applied Physics* 81, 594–600.
- Marques, M. J., Pina, J., Dias, A. M., Lebrun, J. L., Feugeas, J., 2005. X-ray diffraction characterization of ion-implanted austenitic stainless steel. *Surface and Coating Technology* 195, 8–16.
- Matsumura, O., Sakuma, Y., Takechi, H., 1987a. Enhancement of elongation by retained austenite in intercritical annealed 0.4C-1.5Si-0.8Mn steel. *Transactions of the Iron and Steel Institute of Japan* 27, 570–579.
- Matsumura, O., Sakuma, Y., Takechi, H., 1987b. TRIP and its kinetic aspects in austempered 0.4C-1.5Si-0.8Mn steel. *Scripta Metallurgica* 27, 1301–1306.
- McCusker, L. B., Dreele, R. B. V., Cox, D. E., Louer, D., Scardi, P., 1999. Rietveld refinement guidelines. *Journal of Applied Crystallography* 32, 36–50.
- Menapace, C., Lonardelli, I., Tait, M., Moinari, A., 2009. Nanostructured/ultrafine multiphase steel with enhanced ductility obtained by mechanical alloying and spark plasma sintering of powders. *Materials Science & Engineering A* 517, 1–7.
- NPL, 2006. MTDATA. Software, National Physical Laboratory, Teddington, U.K.
- Peet, M., Garcia-Mateo, C., Caballero, F. G., Bhadeshia, H. K. D. H., 2004. Tempering of a hard mixture of bainitic ferrite and austenite. *Materials Science and Technology* 20, 814–818.
- Rietveld, H. M., 1967. Line profiles of neutron powder-diffraction peaks for structure refinement. *Acta Crystallographica* 22, 151–152.
- Rietveld, H. M., 1969. A profile refinement method for nuclear and magnetic structures. *Journal of Applied Crystallography* 2, 65–71.
- Rundman, K. B., Klug, R. C., 1982. X-ray and metallographic studies of an austempered ductile iron. *Transactions of the American Foundrymen Society* 90, 499–508.
- Saha Podder, A., Bhadeshia, H. K. D. H., 2010. Thermal stability of austenite retained in bainitic steels. *Materials Science & Engineering A* 527, 2121–2128.
- Saha Podder, A., Bhattacharjee, D., Ray, R. K., 2007. Effect of martensite on the mechanical behavior of ferrite–bainite dual phase steels. *ISIJ International* 47, 1058–1064.
- Self, P. G., Bhadeshia, H. K. D. H., Stobbs, W. M., 1981. Lattice spacings from lattice fringes. *Ultramicroscopy* 6, 29–40.
- Stone, H. J., Peet, M. J., Bhadeshia, H. K. D. H., Withers, P. J., Babu, S. S., Specht, E. D., 2008. Synchrotron X-ray studies of austenite and bainitic ferrite. *Proceedings of the Royal Society A* 464, 1009–1027.
- Sugimoto, K. I., 2009. Fracture strength and toughness of ultra high strength TRIP aided steels. *Materials Science and Technology* 25, 1108–1117.

Takahashi, M., 1992. Reaustenitisation from bainite in steels. Ph.D. thesis, University of Cambridge, <http://www.msm.cam.ac.uk/phase-trans/2000/phd.html#Takahashi>.

Yates, J. K., 1996. Innovation in rail steel. *Science in Parliament* 53, 2–3.

Yi, H. L., Lee, K. Y., Bhadeshia, H. K. D. H., 2010. Extraordinary ductility in Al-bearing δ -TRIP steel. *Proceedings of the Royal Society A* 467, 234–243.

Proceedings of the Royal Society A 467 (2011) 3141-3156

doi: 10.1098/rspa.2011.0212